Dynamics of Voltage Profile in Enzymatic Ion Transporters, Demonstrated in Electrokinetics of Proton Pumping Rhodopsin

Rolf Hagedorn, Dietrich Gradmann, and Peter Hegemann
Humboldt-Universität zu Berlin, Fachbereich für Biologie, Experimentelle Biophysik, Berlin, Germany

ABSTRACT H^+-pumping rhodopsins mediate a primordial conversion of light to metabolic energy. Bacteriorhodopsin from *Halobacterium salinarium* is the first identified and (biochemically) best-studied H^+-pumping rhodopsin. The electrical properties of H^+-pumping rhodopsins, however, are known in more detail for the homolog *Acetabularia* rhodopsin, isolated from the eukaryotic green alga *Acetabularia acetabulum*. Based on data from *Acetabularia* rhodopsin we present a general reaction kinetic model of H^+-pumping rhodopsins with only seven independent parameters, which fits the kinetic properties of photocurrents as functions of light, transmembrane voltage, internal and external pH, and time. The model describes fast photoisomerization of retinal with simultaneous H^+ transfer to an H^+ acceptor, reprotonation of retinal from the intracellular face via an H^+ donor, and proton release to the extracellular space via an H^+ release complex. The voltage sensitivities of the individual reaction steps and their temporal changes are treated here by a novel approach, whereby—as in an Ohmic voltage divider—the effective portions of the total transmembrane voltage decrease with the relative velocities of the individual reaction steps. This analysis quantitatively infers dynamic changes of the voltage profile and of the pK values of the H^+-binding sites involved.

INTRODUCTION

As for the experimental system, H^+-pumping rhodopsins are the key enzymes for a primordial conversion of light into metabolic energy (i.e., photosynthesis). The crucial, light-driven uphill transport of protons is brought about by a single membrane protein (opsin), which forms the functional entity (rhodopsin) by incorporation of a retinal molecule via a retinylidene Schiff base. Bacteriorhodopsin (BR) from the archaea *Halobacterium salinarium* is the first and biochemically best-investigated rhodopsin (For review, see, e.g., (1)). However, H^+-pumping rhodopsins have also been identified in eubacteria (2), and even eukaryotes (3,4). The electrical properties of light-driven H^+-pumping by rhodopsins were investigated in the past in living cells attached to black-lipid membranes (5–8), in anisotropically suspended rhodopsins in acrylamide gels, in solid supported membranes (9), and in rhodopsins heterologically expressed in oocytes of *Xenopus laevis* (10) or HEK293 cells (11). Steady-state current-voltage relationships could, however, only be recorded in oocytes or HEK293 cells where the rhodopsins are all incorporated with correct orientation and the transmembrane voltage is controlled by the experimenter.

Recently, Tsunoda et al. (3) characterized the light-mediated electrical properties of *Acetabularia* rhodopsin (AR), a rhodopsin from the green alga *Acetabularia*, heterologically expressed in *Xenopus* oocytes. The aim of this study is to understand these properties on a quantitative, physicochemical level by comparing the experimental data with theoretical expectations from appropriate reaction kinetic models. Since the electrical description of AR is more detailed than that of the biochemically and spectroscopically better-investigated bacteriorhodopsin (BR), a discrete model for AR is considered relevant for all H^+ pumping rhodopsins, including BR, of course. The analysis presented here is based on data from a previous study (3). Different methods are available to predict current flow through a transport molecule from the molecular structure of the transport protein. They provide different pros and cons with respect to modeling protein dynamics and description of measured data, whereas MD studies of channels and pumps focus on individual transporter molecules, recordings of whole-cell currents reflect the statistical mean of a larger number of transporters in vivo. To obtain physiologically relevant statements for transmembrane currents from MD, it is necessary, therefore, to calculate means of a larger number of trajectories which is unrealistic at presently available computation facilities, at least in our case of H^+ pumping rhodopsins, where slow relaxations cause additional complications (12). Thus, substantial simplifications are necessary to obtain some macroscopic results from MD. In Brownian dynamics simulations and Poisson-Nernst-Plank approaches a rigid structure of the protein is assumed, and the water molecules are replaced by a continuum (13–15).

In both theories the driving force of an ion i can be described by the Langevin equation $m_i dv = -m_i f_i v_i + F_r + q_i U$, where m_i, q_i, v_i, and f_i are the mass, charge, velocity, and frictional coefficients of the transported species at forces from random collision F_r and a given electric field strength U. To calculate U, Poisson-Nernst-Plank uses the additional simplification that the distribution of ions in the system can be approximated by a continuous charge distribution (13). MD and Brownian dynamics calculations face the problem of accurately determining the (fluctuating) field strength within the channel and great effort has been invested to integrate dielectric

Submitted January 16, 2008, and accepted for publication June 26, 2008.

Address reprint requests to Rolf Hagedorn, Tel.: 49-30-20-93-83-49; E-mail: rolf.hagedorn@rz.hu-berlin.de.

Editor: Francisco Bezanilla.

0006-3495/08/12/5005/09 $2.00

doi: 10.1529/biophysj.107.125260

and mechanical properties into the calculations (14–21). But even if the electric field within the channel were known, it is difficult to get averaged currents from the individual charge trajectories. Another continuum theory that avoids these difficulties is the Nernst-Planck equation which, in our case of H^+ movement, corresponds to Mitchell's concept of protonmotive force (22,23). In fact, structural analysis has revealed proton wells in redox- and light-driven transporters mediating energy conversion (23). The Nernst-Plank approach does not account for noise; instead, it combines Ohm's law for electromigration with Fick's law of diffusion (15,16). If detailed knowledge of the protein structure is not available, these microscopic approaches have to be replaced by macroscopic ones with the assumption that the ions are preferentially localized in specific sites of the pathway and that transitions between these sites determine the kinetics of the global transport process (13). These transitions comprise not only changes of H^+ from one site to an immediately adjacent one, but also migration of H^+ along proton wires (24), including stretches of water networks (25) which are essential not only in energy conversion but also in voltage gating of ion channels by motion of the S4 helix (26–28) and in cotransporters (29,30). To satisfy microscopic and macroscopic aspects of H^+ pumping by rhodopsin, Ferreira and Bashford (31) used an intermediate approach, defining 25 microstates that are linked by conformation changes and proton transfer steps, as determined from molecular dynamic calculations. Here we reduce the structural information even more, namely to an extent that allows a one-to-one assignment to the electrophysiological data available.

The initial aim of this study was an enzyme kinetic analysis of light-induced electrical currents I in H^+ pumping rhodopsins. When conventional reaction kinetic attempts failed, a surprisingly simple modification resulted in a good description of the experimental data. This modification is based on the idea that—like in an Ohmic voltage divider—for each reaction step i, the individual portion $d_i = E_i/E$ of the total voltage, $E = \sum E_i$, decreases with the particular electrical conductance of this step, which, in turn, increases with the rate constants k_i involved. This approach infers considerable temporal changes of the voltage profile within the charge-translocating enzyme upon changes of the conditions, especially of the light intensity. To our knowledge, it is a novel approach to determine d from k, in enzyme kinetics of voltage-dependent transporter proteins.

MATERIALS AND METHODS

Experimental data

The experimental data used here are representative examples from a previous study (3), where statistical support of these data is given.

Model

We adopt the established description of the transport process by a series of transitions of H^+ from one binding site to another (1,32–36). Spectroscopic and crystallographic studies show that the photocycle of BR comprises several small steps of H^+ translocation that add up to a movement of one H^+ through the entire membrane. These reactions, which are the consequences of changes in H^+ affinity of the individual H^+-binding sites, are summarized in Eq. 1, where the main line marks the individual states and reactions. The top line marks the spectroscopic transitions according to the traditional nomenclature, and the bottom line marks the temporal order of the individual steps from Balashov et al. (37):

$$H_i \underset{4}{\xrightarrow{N\to O}} D \underset{3}{\xrightarrow{M\to N}} S \underset{1}{\xrightarrow{BR\to L}} A \underset{5}{\xrightarrow{O\to BR}} C \underset{2}{\xrightarrow{L\to M}} H_o. \quad (1)$$

This scheme reflects the sequence of spectroscopically identified intermediates of the photochemical reaction cycle of BR. It starts with a photoisomerization ($BR \rightarrow L$) of the Schiff base S and a simultaneous transfer of its proton to the acceptor aspartate, A. The next step ($L \rightarrow M$) corresponds to the release of an H^+ from the proton release complex, C, to the external medium. The following transition ($M \rightarrow N$) reflects the H^+ transfer from the donor aspartate, D, to the Schiff base, S. The cycle ends with the spectroscopically identified transitions $N \rightarrow O$ and $O \rightarrow BR$, which reflect the reprotonation of D from the cytoplasmic medium, and the H^+ transfer from the acceptor, A, to the proton release complex, C, respectively. Interestingly, as the behavior of the pump is controlled by transient pK changes (38), the temporal order of these reaction steps differs from their spatial order from inside to outside.

We consider a population of rhodopsin molecules. In this macroscopic view, means of discontinuous molecular events result in apparent continuous functions; e.g., transition probabilities appear as rate constants and mixtures of discrete states as intermediates. Fig. 1 compares some structural features (Fig. 1, *A* and *B*) and a reaction scheme (Fig. 1, *C* and *D*) of H^+ pumping rhodopsins according to the literature (33,39); see also Eq. 1. The left panels (Fig. 1, *A* and *C*) represent the state of a previous study on AR (3), and the right panels (Fig. 1, *B* and *D*) show basically the same features, but with the following updates: The Schiff base, S, is not represented by four states (namely S_o, S_i, S_iH, and S_oH in Fig. 1 *C*), discriminating between orientation toward cytoplasmic and lumenal side (Fig. 1 *C*), but by two states only (S, SH; Fig. 1 *D*), a protonated (resting) state and a deprotonated state. This simplification is justified because vectorial transport can take place without switching accessibility (31,40). Furthermore, the two proton transfer steps from the Donor, D, to S and from the acceptor, A, to the H^+ release complex, C, which has not been considered before, are assumed to be limited by electrodiffusion of H^+ through water network stretches of ~10 Å distance within the H^+ conducting pore, marked by large dots in Fig. 1 *D*. The proton release complex, C, is represented in Fig. 1 *B* by three encircled amino acids (41).

Common entities of the previous model and the model presented here are a voltage-sensitive proton equilibrium between the cytoplasmic bulk phase (H_i) and at the binding site (H_D) of the donor, and protonated/deprotonated states D, S, A of the series of H^+ transfer sites. The rate equations related to the individual steps in Eq. 1 are as follows:

$$\text{Reaction 4}: \quad H_i + D \rightleftharpoons DH, \text{ fast equilibration with } pK_i, \quad (2)$$

$$\text{Reaction 3}: \quad DH + S \rightleftharpoons D + SH, \text{ electromigration with } k_D, \quad (3)$$

$$\text{Reaction 1}: \quad SH + A \rightharpoonup S + AH, \text{ light-driven } H^+\text{-transfer with } k_S, \quad (4)$$

$$\text{Reaction 5}: \quad AH + C \rightleftharpoons A + CH, \text{ electromigration with } k_A, \quad (5)$$

$$\text{Reaction 2}: \quad CH \rightleftharpoons C + H_o, \text{ fast equilibria with } pK_{o1}, pK_{o2}. \quad (6)$$

Equation 2 defines the fast equilibria of protonation on the entrance side, i.e., $D_H/D = 10^{pK_i - pH_i}$. Equation 6 reflects a more complex situation. The

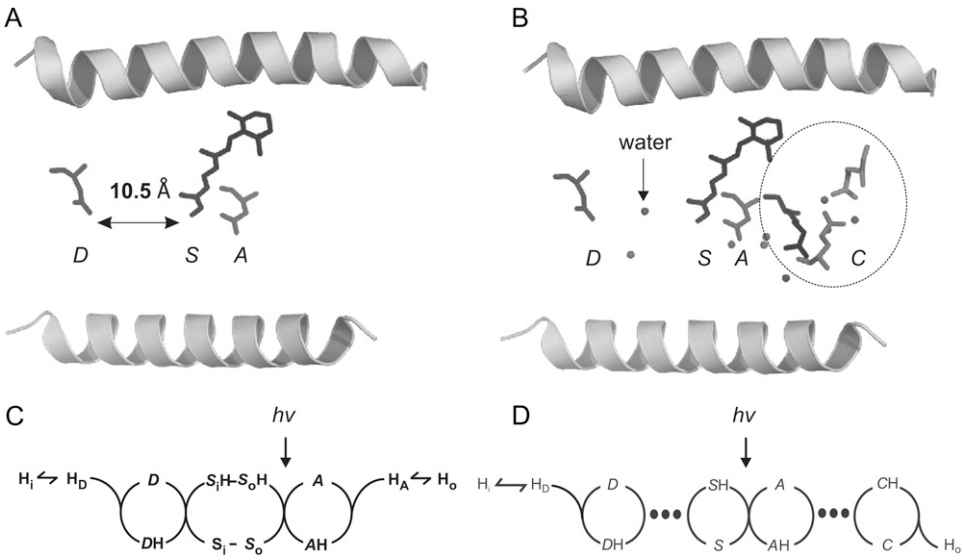

FIGURE 1 Structural (*top*) and kinetic (*bottom*) minimum model for H^+ pumping rhodopsins; left panels (*A* and *C*): preceding three-cycles model in Tsunoda et al. (3), with slightly modified nomenclature; right panels (*B* and *D*): present four-cycles model, extended by stretches of electrodiffusion of H^+ through water (*dots*), and the known proton release complex *C* (35). Symbols: Two schematic helices mark pore, *i*, inside (cytoplasmic space); *o*, outside (luminal space); *D*, proton-donor amino acid in inner half-pore (*D*96 in BR and *D*100 in AR); *S*, Schiff base of photoisomerizing retinal, if indexed; *i*,*o*, access of proton binding site to *D*, *A*, respectively; *A*, proton-acceptor amino acid in outer half-pore (*D*85 in BR and *D*91 in AR); *C*, proton release complex; *Y*57, *R*82, *Y*83, *D*85, *D*96, *E*204 and *D*212 in BR, and *Y*60, *R*86, *Y*87, *D*89, *D*100, *E*206, and *D*214 in AR; H, H^+. Double-headed arrows mark fast H^+ equilibria.

proton-release complex consists of at least three amino acids in BR and is not identified in detail in AR. However, the kinetic effect of pH_o in AR can be accounted for by two different proton acceptors with pK_{o1} and pK_{o2}. Equation 6 represents the averaged protonation of two equilibria, which is $C_H/C = 0.5(10^{pK_{o1}-pH_o} + 10^{pK_{o2}-pH_o})$. Since the relationships between *D* and *D*H as well as those of *C* and *C*H are fixed by the pH- and pK-values for the respective fast equilibria, and since the small transport steps through both water cavities (Eqs. 3 and 5) are merged into only two equations, the system of the Eqs. 2–6 consists of only the two pairs of variables *S*/*S*H and *A*/*A*H. If the net fluxes of the respective reactions 3–5 were denoted as $J_D = J_{DH\rightarrow SH}$, $J_S = J_{SH\rightarrow AH}$, and $J_A = J_{AH\rightarrow CH}$, then the following differential equations describe the changes of the occupation probabilities P_S and P_A of the protonated states *S*H and *A*H,

$$\frac{dP_S}{dt} = J_D - J_S, \tag{7}$$

$$\frac{dP_A}{dt} = J_S - J_A, \tag{8}$$

with

$$J_D = k_D P_{DH} P_S - k_{-D} P_D P_{SH}, \tag{9}$$

$$J_S = k_S P_{SH} P_A - k_{-S} P_S P_{AH}, \tag{10}$$

$$J_A = k_A P_{AH} P_C - k_{-A} P_A P_{CH}, \tag{11}$$

where k_S in Eq. 10 is proportional to the light intensity (see Table 1). Each step of the reaction scheme of Fig. 1 *D* comprises the unidirectional flux $J_i = J_{i\rightarrow i+1}$ of H^+ from one position, *i*, to the next, $i + 1$, through a certain portion of the membrane. In a generalized form, Eqs. 9–11 can be written as

$$J_i = k_i P_i(1 - P_{i+1}) - k_{-i} P_{i+1}(1 - P_i), \tag{12}$$

where i = D, S, or A; P_i is the probability to find a binding site in its protonated form; $(1 - P_i)$ is the probability of a site to be deprotonated; and $k_i = k_{i,i+1}$ and $k_{-i} = k_{i+1,i}$ are the rate constants for the forward and backward transitions.

According to rate theory (42), the portion d_i of the total, reduced transmembrane voltage $u = eE/kT$ will affect the transition probabilities by the relationships

$$k_i = k_i^0 \exp(d_i u/2) \quad k_{-i} = k_{-i}^0 \exp(-d_i u/2), \tag{13}$$

where the superscript 0 marks the *k* value at zero voltage, and the factor 1/2 in the exponents reflect the assumption of a symmetric barrier. For small values of $d_i u$ (linearity) and for $k_i^0 = k_{-i}^0$, Eq. 13 degenerates to

$$k_i = k_i^0(1 + d_i u/2) \quad k_{-i} = k_i^0(1 - d_i u/2). \tag{14}$$

Here we use $k_i^0 = k_{-i}^0$ because electromigration through the water network is assumed symmetric and rate-limiting compared to the fast binding and debinding reactions to and from the corresponding acceptors and donors. Voltage-sensitivities enter Eqs. 9 and 11 by the linear relationships of Eq. 14 for the electromigration of H^+ through a water network. In contrast, the voltage-sensitivity of the direct H^+ transfer from *S*H to *A*H by k_S (Eq. 4) turned out to be better described by the nonlinear formalism of Eq. 13 for an Eyring barrier. In principle, the description of voltage-dependent transition k_i requires two parameters, the height, $1/k_i^0$, and the relative width, d_i, of the barriers within the total voltage profile. However, in an Ohmic sense, these two parameters are not independent, because the partial voltage drop $d_i E$ across the resistor $R_i = 1/G_i$ (G_i = conductance) of a series of resistors with a

TABLE 1 Critical parameters for electrokinetic properties of H^+-pumping rhodopsin; definitions in Fig. 1 *D* and Eqs. 2–6

Symbol	Meaning	Unit	Value	Eqs.	Fig.
pK_i	Equilibrium $H_i^+ \leftrightarrow H^+$, donor.		7.1	2	5
pK_{o1}	1. Equilibrium $H_o^+ \leftrightarrow H^+$, release complex.		3.6	6	5
pK_{o2}	2. Equilibrium $H_o^+ \leftrightarrow H^+$, release complex.		10	6	5
k_D^0	Electrodiffusion $D \leftrightarrow S$ at $E = 0$.	s^{-1}	39	3,14	3,4,5
k_S^0	Photoisomerizing $S \rightarrow A$ at $E = 0$; 100% light.	s^{-1}	≥220	4,13	3,4,5
k_A^0	Electrodiffusion $A \leftrightarrow C$ at $E = 0$.	s^{-1}	65	5,14	3,4,5
d_{Hi}	Fraction in $H_D = H_i \times \exp(d_{Hi}u)$.		0.24	1,6	

total resistance R will be determined by $d_i = R_i/R$, where the velocity k_i^0 may be considered proportional to $1/R_i$. So a relationship $k_i^0\ d_i = const$ might be stated, which would mean that the shape of a barrier is conserved, because lowering its height, $1/k_i^0$, will cause a concomitant narrowing of its width, d_i. In our case, the situation is more complicated, because the conductance equivalent G_i of a reaction step is not only determined by the reference rate constants, k_i^0, but by the actual rate constants k_i, and the occupancies P_i involved. The local current related to charge movement between sites i and $i + 1$ is

$$I_i = eJ_i. \tag{15}$$

The slope conductivity ($G_i = d(I_i)/d(E_i)$) related to the individual reaction steps can be calculated from Eqs. 12 and 15,

$$G_i = \frac{e}{kT}(k_i\ P_i(1 - P_{i+1}) + k_{-i}P_{i+1}(1 - P_i)), \tag{16}$$

where not only the transition probabilities k are important but also the occupancies of the states which can deliver and receive a H^+. With $E_i = G_i I_i$ being the fraction of the electrical potential dropping between site i and site $i + 1$,

$$d_i = E_i/E = \frac{eJ_i}{G_i E}. \tag{17}$$

The Ramo-Shockley theorem (43) states that each process comprising a movement of charge ze within a membrane by the (electric) distance d_i perpendicular to its surface will create corresponding changes of the image charges at the membrane surfaces, which will be recorded under voltage-clamp conditions as the unidirectional current

$$I = \sum d_i I_i \text{ with } i = D, S, \text{ or } A. \tag{18}$$

The kinetic model used here consists of the five reactions in Eqs. 2–6. To reduce the number of independent system parameters to a minimum, the following simplifications are used:

Simplification 1

Reactions 2 and 6 are considered to be fast equilibria which are described by three pK values, one (pK_i) for reaction 2 and two (pK_{o1} and pK_{o2}) for reaction 6. The second equilibrium, pK_{o2} was introduced to satisfy the striking conductance increase at very alkaline pH_o (3). Since a conductance G cannot be calculated from pK values, the fraction d_{Hi} for reaction 2 was calculated from $\sum d_i = 1$. We used this value both for light and dark reactions. A corresponding fraction $d_{Ho} > 0$ for reaction 6 did not improve the fits. Therefore, d_{Ho} could be ignored which resulted in the four parameters pK_i, pK_{o1}, pK_{o2}, and d_{Hi} for the description of these equilibria.

Simplification 2

The light-dependent reaction k_S (reaction 4) can be assumed to be irreversible, i.e., the rate constant k_{-S} for the back-reaction is zero (the blue-light induced exception presented in reaction 3 is not treated here). Since the relative velocity of the forward reaction k_S (compared to the dark reactions k_A and k_D) determines also the electrical distance d_S by Eqs. 16 and 17, reaction 4 is determined by one parameter only k_S, which also represents the light-sensitivity of the system.

Simplification 3

Reactions 3 and 5 describe the migration of a proton through a water network with the linear voltage-dependencies of Eq. 14. This linear approach corresponds to a series of transitions across barriers of similar height. Since the rate constants for forward- and back-reaction can be assumed to be the same at zero voltage, only one system parameter is required for each of these two reactions ($k_A^0 = k_{-A}^0$ and $k_D^0 = k_{-D}^0$) and the fractions, d_A and d_D, are determined again by Eqs. 16 and 17. So these two reactions for electromigration are determined by two additional system parameters altogether.

Summarizing, the entire system can be described by seven system parameters. A scaling factor may be required as an eighth parameter, which accounts for the particular expression level (number of operating rhodopsin molecules) in the oocyte used. This number is in the range of 10^{10} per oocyte (3) and cancels out when experimental data from different oocytes are normalized. An example of this estimate can be obtained by comparing the experimental steady-state photocurrents of $\sim 2 \times 10^{-7}$A from an oocyte in Fig. 2 with the microscopic steady-state currents of an individual rhodopsin in Fig. 4 of $\sim 200\ e\ s^{-1} \approx 3.2 \times 10^{-17}$A with $e \approx 1.6 \times 10^{-19}$A s.

Numerical methods

The electrical behavior is described by means of Eq. 18 with d_i from Eq. 17, and I_i from Eq. 15. The meanings of k_i, G_i, and J_i are defined by Eqs. 9–11, 13, and 16. Calculating the electrical distances, d_i, by Eq. 17 requires the knowledge of G_i and the rate constants $k_i(d_i)$. Therefore, preliminary k_i values were calculated from estimated d_i values first. Using these start values, the values of d_i and k_i were then improved iteratively.

Custom-tailored software was written in C# and is available on request. Model calculations were performed by application of a conventional Runge-Kutta algorithm to Eqs. 7 and 8 and calculation of the least-square error to all data of Figs. 3–5, simultaneously. For fits, the error was minimized by direct search calculations under variation of the model parameters by small steps $<1\%$ per iteration, according to Hookes and Jeeves (44). Suitable start parameters were chosen by trial and error.

RESULTS

Seven independent parameters

Fig. 2 shows a typical example of the time course of photocurrents upon a rectangular light pulse and the measured parameters which can be extracted from such records. In principle, the time course provides five independent observable parameters: the three amplitudes a, b, and c and the two time constants τ_1 and τ_3, respectively, resulting in four parameters

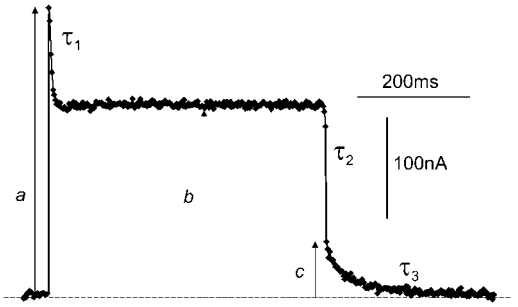

FIGURE 2 Typical time course of photocurrent upon a rectangular light pulse, mediated by a H^+ pumping rhodopsin expressed in *Xenopus* oocytes. Characteristic, observable parameters are the amplitudes: a, initial, fast response; b, steady-state level; and c, initial current after downstep at end of light pulse. Time constants: τ_1 for exponential relaxation from a to b; and τ_3 for exponential relaxation from c to baseline, i.e., dashed control (zero) current in absence of light. Fast changes by τ_0 (from baseline to a, not marked) and τ_2 (from b to c) are not resolved (data from (3)).

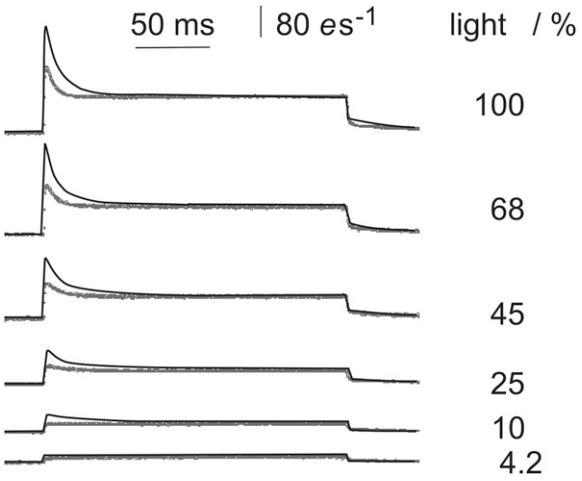

FIGURE 3 Fit to time courses of photocurrents upon square-waved light pulses of different intensity. Currents I are expressed as elementary charges e per second through one rhodopsin molecule. (*Light tracing*) Measured data. (*Dark tracing*) Data fitted by the reaction scheme in Fig. 1 *D* with parameters listed in Table 1. Light intensities as indicated, 100% $\approx 10^{21}$ photons (532 nm) m^{-2} s^{-1}; conditions, $pH_i = 7.3$, $pH_o = 7.3$, and $E = 60$ mV.

when the amplitudes are normalized. The initial currents (a) and the amplitude (c) are determined by extrapolating the following current relaxations to time zero. Therefore, the temporal changes upon the very beginning (τ_0, not drawn) and end of the light pulse (τ_2, not drawn) are not considered here because they are faster than the apparatus could resolve. Corresponding records with different light-intensities and holding voltages, as well as changes of external and internal pH, provide sufficient data to determine the seven system parameters.

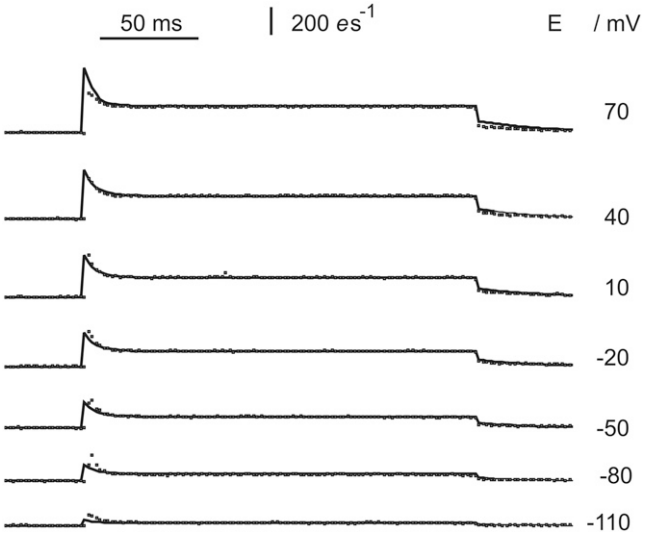

FIGURE 4 Examples of photocurrents upon pulses of green 532 nm light (50 ms bars), recorded at different holding voltages as marked. The points (*light tracings*) are measured and the black curves are fitted by the model described. In Fig. 1 *D* and Eqs. 5–18 with parameters listed in Table 1. Currents I are expressed as elementary charges e per second through one rhodopsin molecule.

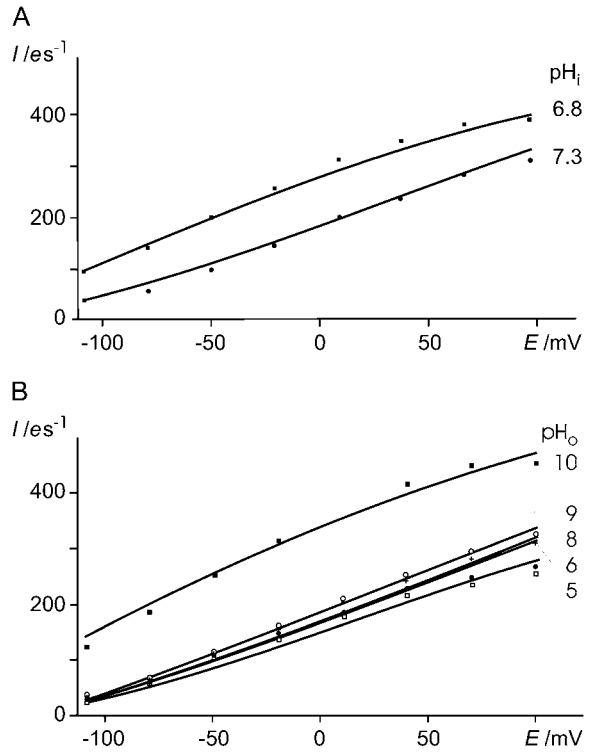

FIGURE 5 (*A*) Sensitivity of steady-state photocurrent (100% light) to transmembrane voltage, E, and to cytoplasmic $[H^+]_i$, pH_i 7.3 and 6.8; points measured, curves calculated by the reaction scheme in Fig. 1 *D* and Eqs. 5–18 with parameters listed in Table 1. (*B*) Sensitivity of steady-state photocurrent (100% light) to transmembrane voltage, E, and to external $[H^+]_o$, pH_o between 4 and 10; points measured, curves calculated by the reaction scheme in Fig. 1 *D* and Eqs. 5–18 with parameters listed in Table 1. Currents I are expressed as elementary charges e per second through one rhodopsin molecule. (*A*) $pH_o = 7.3$, (*B*) $pH_i = 7.3$.

Light titration

The relationships between light intensity and the amplitudes a and b (Fig. 2) of the photocurrents have been described in detail by Tsunoda et al. (3). Fig. 3 shows a typical set of such records. The theoretical records calculated by the model with the parameters in Table 1 are illustrated as black curves in Fig. 3 superimposed to the experimental data in gray. This figure shows that the basic observations are reproduced by the calculations, especially that the light-sensitivity of a is steeper than that of b, which causes the initial peak of the photocurrents to be more pronounced at increasing intensities. As can been seen from Fig. 3, the time constant τ_1 is underestimated by our model fits. We ascribe these differences to an insufficient temporal resolution of the recording apparatus: Faster τ_1-constants would improve the fit quality but would result in initial peaks much too high to be resolved by the apparatus.

Voltage sensitivity

Measurements and fits of the time course of photocurrents at different holding voltages are shown in Fig. 4. Interestingly, the ratio a/b (i.e., the ratio between the initial amplitude a and

the steady-state amplitude, b; see Fig. 2) increases with the absolute level of b. This feature is reproduced by the model, although not as pronounced as in the experimental records. The voltage-dependence of the steady-state currents, i.e., steady-state $I(E)$ curves are represented in more detail by Fig. 5, together with the impact of external and internal pH.

At a first glance, the sections of $I(E)$ curves in Fig. 5 may appear quite linear. However, the irreversibility of reaction 6 renders negative photocurrents impossible. They rather approach zero at very negative E. As for the positive voltage range, the experimental data show only a weak tendency for saturation. Also, in this model, currents are not limited for large positive voltages; instead, they approach an asymptote of a finite slope of $k_D d_D \approx k_A d_A$, where k_D and k_A rise proportional with u (Eq. 14), $P_{D,A} \rightarrow 1$, and d_A, d_D approach finite values.

pH sensitivity

Fig. 5, *A* and *B*, show the sensitivities of the steady-state currents (b) to clamp-voltages and to the concentrations of the substrate at both sides of the membrane (cytoplasmic $[H^+]_i$, pH_i) and to the external $[H^+]_o$, (pH_o)). Since the internal volume of the oocyte is not freely accessible, the changes in pH_i cover only half a pH unit (Fig. 5 *A*). Nevertheless, the effect of pH_i is strong, as expected for substrate-dependence. In more detail, the fits of the model to the data show a good coincidence and result in a pK_i of 7.1 (Table 1, Fig. 5 *A*). This means that under high light conditions, the supply of H_i controls the pump current. In contrast, the sensitivity of the steady-state current-voltage relationship to the external proton concentration, $[H^+]_o$, is weak (Fig. 5 *B*). This is expected for an enzyme operating far from equilibrium. According to the model, the increased pumping rates observed at alkaline pH_o is due to the proton release complex (*C*) and the protonation state of the participating amino-acid side chains. Fig. 5 *B* shows current changes by only a few %, per pH unit between pH_o 4 and pH_o 9, which is readily fitted by a $pK_o = 3.6$ for the equilibration of the proton release complex (*C*). However, the observed increase of the current at pH_o 10 cannot be explained by an acceptor with pK_{o1} 3.6. The fair coincidence of fit and data at pH_o 10 in Fig. 5 *B* could only be accomplished by the assumption of another amino acid of the proton release complex that causes equilibration with the external medium with $pK_{o2} \approx$ 10. Arg^{86} in AR is a likely candidate corresponding to Arg^{82} in BR. The curvature of the fitted curve of the model to the pH_o 10 in Fig. 5 *B* is not strong enough to match the experimental data perfectly. It should be noted at this point that the current-voltage curve of BR does not show such a pronounced curvature (11) and that the entire proton release complex is represented here by two amino acids only.

Voltage profile

The three H^+ flux components ($J_D = J_{DH \rightarrow SH}$, Eq. 9; $J_s = J_{SH \rightarrow AH}$, Eq. 10; and $J_A = J_{AH \rightarrow CH}$, Eq. 11) as they result from this analysis, are plotted separately in Fig. 6 *B*. The serial arrangement of the fluxes (see Fig. 6) lead to the same steady-state value for each flux, whereas characteristic differences in the temporal behavior are assessed. Fig. 6 *C* shows steady-state values of the electric distances $d_D \approx 0.27$, $d_S \approx 0.38$, and $d_A \approx 0.11$, which were determined from Eqs. 13, 14, and 16–19, iteratively, as described above, whereas the value of d_{Hi} defines the voltage- and pH_i sensitivity of reaction 2. During illumination the value $d_{Hi} = 0.24$ follows from $\sum d_i = 1$. We use the same value as an approximation for the dark reaction. The relationship between these steady-state values of d_i might also be extracted from the current relaxation after light-off (e.g., Figs. 2 and 3) where the amplitude (b–c) of the immediate decay from b to c reflects the fast kinetics of the light-sensitive component J_S (Fig. 6 *B*), and the amplitude c of the slow component is assigned to the slow kinetics of the components J_D and J_A. Neglecting current-contributions of the fast equilibrium (2) we can estimate from the experimental data $b/c = I_{light}/I_{light\ off} \approx 1/(d_D + d_A) \approx 2.6$.

The implications of the novel approach of a variable voltage profile are illustrated schematically by the lower part of Fig. 6 *A*. This scheme shows that during darkness there is no

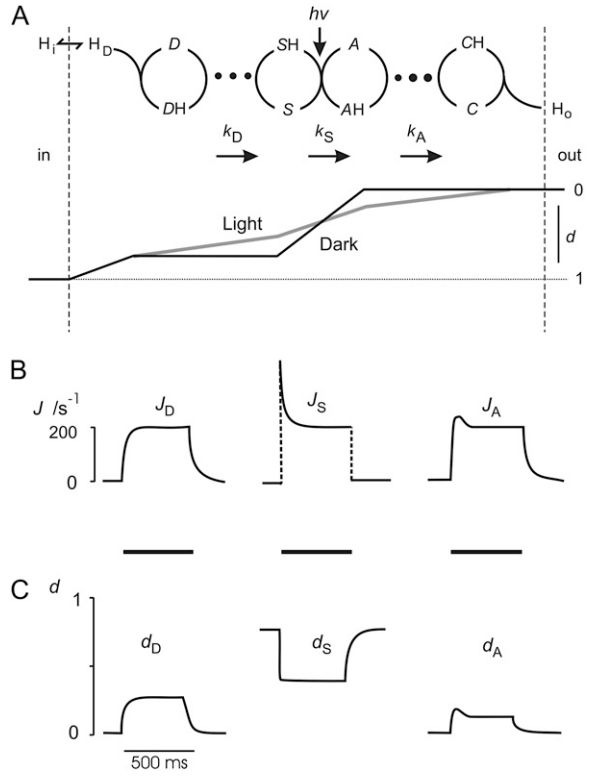

FIGURE 6 Analytical synopsis of light-induced kinetics in H^+ pumping rhodopsins. (*A*) Reaction scheme from Fig. 1 *D* with an illustration of changes in voltage profile u due to changes of electric distances d along the H^+ pathway through rhodopsin under light and dark conditions. (*B*) Time course of the three flux components: J_D, J_S, and J_A upon illumination of rhodopsins with 500 ms pulses of 100% light, at $pH_i = 7.3$, $pH_o = 7.3$, and $E =$ 100 mV, calculated by model with parameters listed in Table 1. (*C*) Time course of the electrical distances d_D, d_S, and d_A under conditions as for panel *B*.

voltage drop across the stretches of H^+ diffusion because of d_D, $d_A = 0$. Upon illumination, the voltage sensitivity coefficients d_D and d_A for k_D and k_A in Eq. 14 become >0 because of the decrease of d_S from its maximum value in darkness. Fig. 6 *C* shows a typical example of the time course of these changes upon a rectangular pulse of bright light. It should be noted that the fits presented here infer explicit changes of d_i as functions of voltage, pH_i, pH_o, light intensity, and time.

DISCUSSION

We do not focus on the experimental data here because they have been discussed before (3). We rather point out some implications of the model for the understanding of the pump mechanism of H^+ pumping rhodopsins.

The main accomplishment of this study is the description of the available electrokinetic data on H^+ pumping rhodopsin at different light, pH, and voltage conditions by an enzyme kinetic reaction scheme which is in line with our spectroscopic and structural knowledge of these membrane proteins. It is clear that the description is not perfect, and does permit future refinements by appropriate extensions. However, the small number of only seven independent parameters for this description of all the data renders the numerical solution unambiguous—within the statistical limits of the experimental data, of course—which is an important benefit.

This design of the model is not the result of a straightforward strategy but the outcome of a long series of ad hoc attempts to find a powerful and satisfying reaction system.

Linear or exponential voltage-sensitivity

The impact of water networks in proton pumping is widely recognized (45) and discussed under various aspects:

1. Water networks can form spontaneously in cavities (46). It can be assumed that in these networks, transport can take place with hardly any barriers by a Grotthus-like mechanism (47).
2. The transfer of a proton between donor and acceptor, located as far as 6–7 A apart, necessitates the participation of water molecules in the process (48).
3. After photoabsorption, energy is partially stored in the form of the weakened hydrogen bonds (49).

It may be asked why the degenerated, linear version Eq. 14 is used to describe the voltage-sensitivity of k_D and k_A, because the nondegenerated, exponential form Eq. 13 can be expected to work equally well. The answer is the following:

First, the mechanism of electrodiffusion through aquatic pores can be assumed to follow the familiar, linear form of the Nernst-Plank equation.

Second, an alternative treatment by Eq. 13 summarizing several small barriers into one, would result in underestimates of the apparent d_i, which would result in the conceptual impossibility of $\sum d_i < 1$. This can be demonstrated by the following example: For one symmetric Eyring barrier of the electrical width 1 between the two bases A and C, the rate constants k_{AC} and k_{CA} for the forward and back reactions will display the voltage sensitivities $k_{AC} = k^0_{AC}\exp(u/2)$ and $k_{CA} = k^0_{CA}\exp(-u/2)$. In case of an intermediate base B in the electrical middle, the gross reactions are $k_{AC'} = k_{ABC} = k_{AB}k_{BC}/(k_{BA} + k_{BC})$ and $k_{CA'} = k_{CBA} = k_{CB}k_{BA}/(k_{BA} + k_{BC})$, and the two barriers over the electrical width of 1/2 each will yield the overall voltage-sensitivity $k_{AC'} = k^0_{AB}\exp(u/4)k_{BC}\exp(u/4)/(k_{AB}\exp(-u/4) + k_{BC}\exp(u/4))$, and the corresponding expression for $k_{CA'}$. Shortening these expressions by $\exp(u/4)$ and ignoring $\exp(-u/4)$ for larger values of u, yields the smaller voltage-sensitivities $k_{AC'} = k^0_{AC'}\exp(u/4)$ and $k_{CA'} = k^0_{CA'}\exp(-u/4)$ with $k^0_{CA'} = k^0_{CB}$, respectively. (In other words, the more barriers over a certain distance, the weaker the voltage-sensitivity of the gross reaction. The extreme case is an Ohmic-linear behavior of hopping electrons over many minute barriers in metallic conductors.)

Third, we employ Eq. 13 instead of Eq. 14 for k_D and k_A. Correspondingly, fits using Eq. 13 instead of Eq. 14 for the voltage-sensitivity of k_D and k_A, resulted in a >50% increase of the mean error. Whether the intrinsically linear slope of the $I(E)$ curves for large positive voltages is correct or not (e.g., saturating, and thus calling for a modification of the model), might be answered by future studies. In particular, the enormous impact of the apparent charge of the empty binding site(s) within an ion transporter (50), needs to be explored here. This model, at least, satisfies the available data.

pK changes

Light-induced pK changes of the H^+ binding sites in rhodopsins are well known (32,35,36). In our model, this is evident for the Schiff base, *S*, due to $k_S = k^0_S \times \mathit{light}$ in the dissociation rate constant k_S. Since the light-induced increase of k_S will cause concomitant changes in the voltage profile (Fig. 6 *A*), k_D and k_A will decrease due to Eq. 14 under physiological conditions of a negative voltage inside. This mechanism is visualized in Fig. 6 *A* by a change of the slopes of the electric field for the rate constants k_A and k_D for H^+ electrodiffusion, from left to right and from neutral to uphill, which will cause an apparent decrease of pK_D and pK_A and an increase of pK_C. The situation of k_S is basically equivalent but more complicated due to its light-sensitivity. This view does not exclude, of course, that light and voltage may change pK values in rhodopsin by steric mechanisms as well. Nevertheless the kinetic mechanism proposed here is a compelling consequence of the model. It is expected that these kinetic pK changes differ between most spectroscopic conditions ($u = 0$) and physiological conditions ($u < 0$).

We thank Dr. Tsunoda for providing files of original experimental data.

This work was supported by the Deutsche Forschungsgemeinschaft (to P.H).

REFERENCES

1. Lanyi, J. K. 2006. Proton transfers in the bacteriorhodopsin photocycle. *Biochim. Biophys. Acta.* 1757:1012–1018.
2. Béjà, O., L. Aravind, E. V. Koonin, M. T. Suzuki, A. Hadd, L. P. Nguyen, S. B. Jovanovich, C. M. Gates, R. A. Feldman, J. L. Spudich, E. N. Spudich, and E. F. DeLong. 2000. Bacterial rhodopsin: evidence for a new type of phototrophy in the sea. *Science.* 289:1902–1906.
3. Tsunoda, S. P., D. Ewers, S. Gazzarrini, A. Moroni, D. Gradmann, and P. Hegemann. 2006. H^+-pumping rhodopsin from the marine alga *Acetabularia*. *Biophys. J.* 91:1471–1479.
4. Waschuk, S. A., A. G. Bezerra, L. Shi, and L. S. Brown. 2005. *Leptosphaeria* rhodopsin: bacteriorhodopsin-like proton pump from a eukaryote. *Proc. Natl. Acad. Sci. USA.* 102:6879–6883.
5. Dancsházy, Z., and B. Karvaly. 1976. Incorporation of bacteriorhodopsin into a bilayer lipid membrane; a photoelectric-spectroscopic study. *FEBS Lett.* 72:136–138.
6. Herrmann, T. R., and G. W. Rayfield. 1976. A measurement of the proton pump current generated by bacteriorhodopsin in black lipid membranes. *Biochim. Biophys. Acta.* 443:623–628.
7. Bamberg, E., N. A. Dencher, A. Fahr, and M. P. Heyn. 1981. Transmembranous incorporation of photoelectrically active bacteriorhodopsin in planar lipid bilayers. *Proc. Natl. Acad. Sci. USA.* 78:7502–7506.
8. Läuger, P., R. Benz, G. Stark, E. Bamberg, P. C. Jordan, A. Fahr, and W. Brock. 1981. Relaxation studies of ion transport systems in lipid bilayer membranes. *Q. Rev. Biophys.* 14:513–598.
9. Heyse, S., O. P. Ernst, Z. Dienes, K. P. Hofmann, and H. Vogel. 1998. Incorporation of rhodopsin in laterally structured supported membranes: observation of transducin activation with spatially and time-resolved surface plasmon resonance. *Biochemistry.* 37:507–522.
10. Nagel, G., B. Möckel, G. Büldt, and E. Bamberg. 1995. Functional expression of bacteriorhodopsin in oocytes allows direct measurement of voltage dependence of light induced H^+ pumping. *FEBS Lett.* 377:263–266.
11. Geibel, S., T. Friedrich, P. Ormos, P. G. Wood, G. Nagel, and E. Bamberg. 2001. The voltage-dependent proton pumping in bacteriorhodopsin is characterized by optoelectric behavior. *Biophys. J.* 81:2059–2068.
12. Grossfield, A., S. E. Feller, and M. C. Pitman. 2007. Convergence of molecular dynamics simulations of membrane proteins. *Proteins.* 67:31–40.
13. Levitt, D. G. 1999. Modeling of ion channels. *J. Gen. Physiol.* 113: 789–794.
14. Moy, G., B. Corry, S. Kuyucak, and S. H. Chung. 2000. Tests of continuum theories as models of ion channels. I. Poisson-Boltzmann theory versus Brownian dynamics. *Biophys. J.* 78:2349–2363.
15. Corry, B., S. Kuyucak, and S. H. Chung. 2000. Tests of continuum theories as models of ion channels. II. Poisson-Nernst-Planck theory versus Brownian dynamics. *Biophys. J.* 78:2364–2381.
16. Schuss, Z., B. Nadler, and R. S. Eisenberg. 2001. Derivation of Poisson and Nernst-Planck equations in a bath and channel from a molecular model. *Phys. Rev. E Stat. Nonlin. Soft Matter Phys.* 64:036116.
17. Corry, B., S. Kuyucak, and S.-H. Chung. 2003. Dielectric self-energy in Poisson-Boltzmann and Poisson-Nernst-Planck models of ion channels. *Biophys. J.* 84:3594–3606.
18. Nadler, B., U. Hollerbach, and R. S. Eisenberg. 2003. Dielectric boundary force and its crucial role in gramicidin. *Phys. Rev. E Stat. Nonlin. Soft Matter Phys.* 68:021905.
19. Zhang, J., A. Kamenev, and B. I. Shklovskii. 2005. Conductance of ion channels and nanopores with charged walls: a toy model. *Phys. Rev. Lett.* 95:148101.
20. Cherstvy, A. G. 2006. Electrostatic screening and energy barriers of ions in low-dielectric membranes. *J. Phys. Chem. B.* 110:14503–14506.
21. Hoyles, M., V. Krishnamurthy, M. Siksik, and S.-H. Chung. 2008. Brownian dynamics theory for predicting internal and external blockages of tetraethylammonium in the KcsA potassium channel. *Biophys. J.* 94:366–378.
22. Mitchell, P. 1961. Coupling of phosphorylation to electron and hydrogen transfer by a chemi-osmotic type of mechanism. *Nature.* 191:144–148.
23. Mulkidjanian, A. Y. 2006. Proton in the well and through the desolvation barrier. *Biochim. Biophys. Acta.* 1757:415–427.
24. Nagle, J. F., and H. J. Morowitz. 1978. Molecular mechanisms for proton transport in membranes. *Proc. Natl. Acad. Sci. USA.* 75:298–302.
25. Jogini, V., and B. Roux. 2007. Dynamics of the $Kv_{1.2}$ voltage-gated K^+ channel in a membrane environment. *Biophys. J.* 93:3070–3082.
26. Bezanilla, F. 2000. The voltage sensor in voltage-dependent ion channels. *Physiol. Rev.* 80:555–592.
27. Bezanilla, F. 2005. The voltage-sensor structure in a voltage-gated channel. *Trends Biochem. Sci.* 30:166–168.
28. Starace, D. M., and F. Bezanilla. 2004. A proton pore in a potassium channel voltage sensor reveals a focused electric field. *Nature.* 427:548–553.
29. Abramson, J., I. Smirnova, V. Kasho, G. Verner, H. R. Kaback, and S. Iwata. 2003. Structure and mechanism of the lactose permease of *Escherichia coli*. *Science.* 301:610–615.
30. Arkin, I. T., H. Xu, M. Ø. Jensen, E. Arbely, E. R. Bennett, K. J. Bowers, E. Chow, R. O. Dror, M. P. Eastwood, R. Flitman-Tene, B. A. Gregersen, J. L. Klepeis, I. Kolossváry, Y. Shan, and D. E. Shaw. 2007. Mechanism of Na^+/H^+ antiporting. *Science.* 317:799–803.
31. Ferreira, A. M., and D. Bashford. 2006. Model for proton transport coupled to protein conformational change: application to proton pumping in the bacteriorhodopsin photocycle. *J. Am. Chem. Soc.* 128:16778–16790.
32. Spassov, V., and D. Bashford. 1998. Electrostatic coupling to pH-titrating sites as a source of cooperativity in protein-ligand binding. *Protein Sci.* 7:2012–2025.
33. Luecke, H., B. Schobert, H. T. Richter, J. P. Cartailler, and J. K. Lanyi. 1999. Structural changes in bacteriorhodopsin during ion transport at 2 Ångstrom resolution. *Science.* 286:255–261.
34. Miller, C. 1999. Ionic hopping defended. *J. Gen. Physiol.* 113:783–787.
35. Spassov, V. Z., H. Luecke, K. Gerwert, and D. Bashford. 2001. pK_a Calculations suggest storage of an excess proton in a hydrogen-bonded water network in bacteriorhodopsin. *J. Mol. Biol.* 312:203–219.
36. Edman, K., A. Royant, G. Larsson, F. Jacobson, T. Taylor, D. van der Spoel, E. M. Landau, E. Pebay-Peyroula, and R. Neutze. 2004. Deformation of helix C in the low temperature L-intermediate of bacteriorhodopsin. *J. Biol. Chem.* 279:2147–2158.
37. Balashov, S. P., M. Lu, E. S. Imasheva, R. Govindjee, T. G. Ebrey, B. Othersen, Y. Chen, R. K. Crouch, and D. R. Menick. 1999. The proton release group of bacteriorhodopsin controls the rate of the final step of its photocycle at low pH. *Biochemistry.* 38:2026–2039.
38. Balashov, S. P. 2000. Protonation reactions and their coupling in bacteriorhodopsin. *Biochim. Biophys. Acta.* 1460:75–94.
39. Luecke, H., B. Schobert, H. T. Richter, J. P. Cartailler, and J. K. Lanyi. 1999. Structure of bacteriorhodopsin at 1.55 Å resolution. *J. Mol. Biol.* 291:899–911.
40. Bondar, A.-N., J. C. Smith, and S. Fischer. 2006. Structural and energetic determinants of primary proton transfer in bacteriorhodopsin. *Photochem. Photobiol. Sci.* 5:547–552.
41. Kandt, C., J. Schlitter, and K. Gerwert. 2004. Dynamics of water molecules in the bacteriorhodopsin trimer in explicit lipid/water environment. *Biophys. J.* 86:705–717.
42. Bard, A. J., and L. R. Faulkner. 2001. Electrochemical Methods, Fundamentals and Applications, 2nd Ed. John Wiley & Sons, New York, Chichester, Weinheim, Brisbane, Singapore, Toronto.

43. Nonner, W., A. Peyser, D. Gillespie, and B. Eisenberg. 2004. Relating microscopic charge movement to macroscopic currents: the Ramo-Shockley theorem applied to ion channels. *Biophys. J.* 87:3716–3722.

44. Hookes, R., and T. Jeeves. 1961. Direct search solution of numerical and statistical problems. *J. ACM.* 8:212–229.

45. Buch-Pedersen, M., B. Pedersen, B. Veierskov, P. Nissen, and M. Palmgren. 2008. Protons and how they are transported by proton pumps. *Pflugers Arch*. Http://dx.doi.org/10.1007/s00424–008–0503–8.

46. Grudinin, S., G. Büldt, V. Gordeliy, and A. Baumgaertner. 2005. Water molecules and hydrogen-bonded networks in bacteriorhodopsin-molecular dynamics simulations of the ground state and the M-intermediate. *Biophys. J.* 88:3252–3261.

47. Pomès, R., and B. Roux. 1998. Free energy profiles for H^+ conduction along hydrogen-bonded chains of water molecules. *Biophys. J.* 75:33–40.

48. Friedman, R., S. Fischer, E. Nachliel, S. Scheiner, and M. Gutman. 2007. Minimum energy pathways for proton transfer between adjacent sites exposed to water. *J. Phys. Chem. B.* 111:6059–6070.

49. Hayashi, S., E. Tajkhorshid, H. Kandori, and K. Schulten. 2004. Role of hydrogen-bond network in energy storage of bacteriorhodopsin's light-driven proton pump revealed by ab initio normal-mode analysis. *J. Am. Chem. Soc.* 126:10516–10517.

50. Gradmann, D., and C. M. Boyd. 2005. Apparent charge of binding site in ion-translocating enzymes: kinetic impact. *Eur. Biophys. J.* 34: 353–357.